Protist, Vol. 162, 373–393, July 2011
http://www.elsevier.de/protis
Published online date 21 March 2011

Protist

ORIGINAL PAPER

The Ultrastructure of *Ancyromonas*, a Eukaryote without Supergroup Affinities

Aaron A. Heiss[a,b], Giselle Walker[c], and Alastair G.B. Simpson[a,b,1]

[a]Department of Biology, Dalhousie University, Halifax, NS B3H 4J1, Canada
[b]Canadian Institute for Advanced Research, Programme in Integrated Microbial Biodiversity
[c]Department of Earth Sciences, Cambridge University, Cambridge CB2 3EQ, UK

Submitted April 30, 2010; Accepted July 3, 2010
Monitoring Editor: B. S. C. Leadbeater

The small heterotrophic flagellate *Ancyromonas* (=*Planomonas*) lacks close relatives in most molecular phylogenies, and it is suspected that it does not belong to any of the recognized eukaryote 'supergroups', making it an organism of great evolutionary interest. Proposed relatives include apusomonads and excavates, but limited understanding of the ancyromonad cytoskeleton has precluded identification of candidate structural homologies. We present a detailed analysis of the ultrastructure of *Ancyromonas* through computer-based reconstruction of serial sections. We confirm or extend previous observations of its major organelles (mitochondria, Golgi body, extrusomes, etc.) and pellicle, and distinguish a system of stacked endomembranes that may be developmentally connected to the glycocalyx. *Ancyromonas* has two basal bodies, each with its own flagellar pocket. The anterior basal body associates with two microtubular elements: a doublet root that runs from between the basal bodies to support the cell's rostrum, and a short singlet root. The posterior basal body is associated with two multi-microtubular structures and a singlet root. One multi-microtubular structure, L1, is a conventional microtubular root. The other structure appears as a curved ribbon of ~8 microtubules near the basal body, but then flares out into two multi-microtubular elements, L2 and L3, plus two single microtubules. The posterior singlet root originates independently near this second complex. L1, the singlet, L2, and L3 all support the posterior flagellar pocket and channel. We also identified several groups of peripheral microtubules. Possible homologies with the flagellar apparatus of both apusomonads and excavates include a splitting root on the right side of the posterior basal body and a singlet root, both supporting a longitudinal channel or groove associated with the posterior flagellum. The anterior flagellar apparatus in each includes a root supporting structures to the left of the anterior flagellum. Given the probable deep divergences of *Ancyromonas*, apusomonads and excavates within eukaryotes, it is possible that the eukaryotic cenancestor also possessed these features.

Key words: Apusozoa; cytoskeleton; electron microscopy; evolution; flagellar apparatus; protozoa.

Introduction

Most eukaryotic organisms are currently thought to belong to one or another of four to six 'supergroups'. While controversies persist regarding this arrangement, it has proven a reasonable point of reference and a viable working model (Adl et al. 2005; Baldauf 2003; Burki et al. 2007, 2008; Cavalier-Smith 2009; Hampl et al. 2009; Keeling et al. 2005; Simpson and Roger 2004). Much recent work has focused on determining whether the

[1]Corresponding author. Fax: +1 902 494 3736.
e-mail alastair.simpson@dal.ca (A.G.B. Simpson).

doi:10.1016/j.protis.2010.08.004

supergroups themselves are each monophyletic, what the topology of the tree connecting them is, and the position of the root of the tree. One of the more popular proposals is that the supergroups are divided amongst two even-larger clades: 'unikonts', containing animals, fungi, and most lobose amoebae and slime moulds, and 'bikonts', including all photosynthetic eukaryotes as well as a wide array of protozoa (Cavalier-Smith 2002; Keeling et al. 2005). This hypothesis was supported by gene fusion data (Stechmann and Cavalier-Smith 2002, 2003) and myosin gene family distribution (Richards and Cavalier-Smith 2005), and is consistent with unrooted multigene phylogenies (Burki et al. 2007, 2008; Hampl et al. 2009). It is however very much a tentative hypothesis, in the absence of other molecular characters, reliably rooted phylogenies, or convincing morphological data (Arisue et al. 2005; Parfrey et al. 2006; Roger and Simpson 2009; Simpson and Roger 2004; Yoon et al. 2008).

Nonetheless, the relationships among the supergroups, as currently recognized, give only an incomplete picture of eukaryote history. Several 'orphan' groups exist that do not fit into any of the established supergroups (Simpson and Roger 2004). Placing these orphan groups could help us resolve deep-level eukaryotic phylogeny and may well be essential for a clear understanding of early eukaryote evolution (Cavalier-Smith 2009; Minge et al. 2009; Patterson 1999; Patterson et al. 2000).

Perhaps the most intriguing orphans are the taxa collected under the name 'Apusozoa'. The core members of Apusozoa are two groups of small heterotrophic gliding biflagellate cells, apusomonads and *Ancyromonas*. The apusomonads include the derived genus *Apusomonas* and the basal and paraphyletic assemblage previously equated with the genus *Amastigomonas* (Cavalier-Smith and Chao 2003; Karpov and Mylnikov 1989), but very recently divided into several new genera (Cavalier-Smith and Chao 2010). The isolated genus *Ancyromonas* (Atkins et al. 2000a,b; Cavalier-Smith 2002) has been studied most recently under the junior synonym *Planomonas* (Cavalier-Smith et al. 2008; Heiss et al. 2010). At various times, this grouping has been proposed to contain other organisms of uncertain affinities including the rotationally symmetrical multiflagellated Hemimastigophora (Cavalier-Smith 2002, 2003) and, most recently, the little-studied amoeboid organism *Micronuclearia* (Cavalier-Smith et al. 2008). Apusozoa are of particular interest to the study of eukaryotic evolution because these organisms show affinities with both unikonts and bikonts (Cavalier-Smith 2009). Apusomonads exhibit the dihydrofolate reductase–thymidylate synthetase gene fusion supposedly characteristic of bikonts (Stechmann and Cavalier-Smith 2003), and some molecular phylogenies place apusozoans amongst bikonts (Cavalier-Smith 2002; Cavalier-Smith and Chao 2003; Cavalier-Smith et al. 2004). Most molecular phylogenies, however, place apusomonads and/or *Ancyromonas* as related to some or all unikonts, albeit often with weak support (Atkins et al. 2000a,b; Cavalier-Smith and Chao 1995; Cavalier-Smith et al. 2004; Kim et al. 2006). Thus, apusozoan lineages could represent deep branches in either the unikont or bikont regions of the tree, or, conceivably, be basal to all other extant eukaryotes.

The importance of Apusozoa to understanding eukaryote evolution is complicated by a number of issues. For one, it is far from proven that apusomonads and *Ancyromonas* constitute a single group. Molecular phylogenies rarely recover apusomonads and *Ancyromonas* as a clade with strong statistical support, and frequently place them as separate deep-branching lineages with no close relatives (Atkins et al. 2000a,b; Cavalier-Smith et al. 2008; Marande et al. 2009). For another, we know relatively little of their cell morphology and biology: even basic ultrastructural studies have been limited to date. Transmission electron microscopy (TEM) data on apusomonads appears in several separate works (Cavalier-Smith and Chao 2003, 2010; Karpov 2007; Karpov and Mylnikov 1989; Karpov and Zhukov 1984, 1986; Molina and Nerad 1991; Mylnikov 1989) but of these, only one recent study of *Apusomonas* includes sufficient data to support a three-dimensional model of the flagellar apparatus (Karpov 2007). Ultrastructural information on *Ancyromonas* is restricted to a general survey of *Ancyromonas sigmoides* by Mylnikov (1990) under the name *Heteromita* sp., four micrographs in Heiss et al. (2010), a limited survey of a second species by Cavalier-Smith et al. (2008), a single micrograph in Cavalier-Smith and Chao (2003), and another micrograph (to show mitochondrial structure) by Mikrjukov and Mylnikov (2001). Solid hypotheses of homology, linking Apusozoa to each other and/or to other eukaryotic groups, await a broader understanding of both apusomonads and *Ancyromonas*.

We present here the first thorough morphological study of *Ancyromonas*, specifically *Ancyromonas sigmoides* strain B-70, from which the neotype for this species was prepared (Heiss et al. 2010). We used serial sectioning and TEM to produce a three-dimensional model of the flagellar apparatus, as well as of much of the cytoskeleton in the rest of the cell. We compare the ultrastructure of

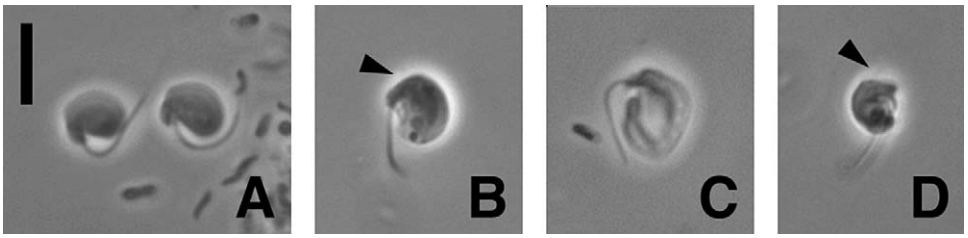

Figure 1. Phase-contrast light micrographs of live cells of *Ancyromonas sigmoides*. **A:** Dorsal view of two cells. The cell on the left is in a typical gliding configuration. Note the extended acroneme of the flagellum on the left cell. **B:** Dorsal view showing the channel immediately posterior to the rostrum as well as several organelles. The nucleus is the largest of these, situated to the right in the image. The anterior flagellum is barely visible (arrowhead). **C:** Dorsal view showing the full extent of the posterior flagellar channel. **D:** Ventral view showing the point of insertion of the posterior flagellum. The anterior flagellum is also visible (arrowhead). Scale bar: 5 μm for all images.

Ancyromonas to apusomonads, as well as to 'typical excavates'.

Results

Overall Morphology

Isolate B-70 of *Ancyromonas sigmoides* is an ovate, kidney-shaped cell, typically 4–5 μm long, 2–4 μm wide (Figs 1A–D, 2A), and dorsoventrally depressed, about 1 μm thick (Fig. 2B). On its left side the cell has a substantial rostrum that contains extrusomes (Figs 1A–D, 2A, C). Separating the rostrum from the main body is a channel running about a third to halfway down the length of the cell. There are two flagella, whose basal bodies are about 80° apart (Fig. 2D). The posterior flagellum is initially directed laterally (Fig. 1D before curving posteriorly (Figs 1A–C). The anterior flagellum is directed anteriorly, but is usually extremely thin for most of its length, extremely short, or both, and thus difficult or impossible to see by light microscopy (Figs 1B, 1D, 2D). Each of the two flagella emerges into a separate flagellar pocket, about 0.5 μm deep (Fig. 2C, D). The anterior flagellar pocket is continuous with a narrow but sharply defined slit that continues to the left, along the rostrum (Figs 2B, 4D). This slit opens into a wider depression into which the extrusomes project (Fig. 4D). The posterior flagellar pocket opens into a posterior channel, which keeps the same width as the pocket (Fig. 4E–4H), unlike the anterior slit.

The ovoid nucleus is located close to the flagellar apparatus (Fig. 2C, D). The subcentral nucleolus is visible only rarely in our preparations (Fig. 2C). Cells can have at least two mitochondria each: we found two distinct mitochondria in half of our eight series of interphase cells, and cannot rule out the possibility that additional mitochondria existed in the same cell outside the range of any of our series (two are visible in Fig. 2C). The mitochondrial cristae are flattened, tending toward discoidal (Figs 2D, 3A), although very broad, flat cristae are also observed (Fig. 2B). Many mitochondria are cup-shaped (Fig. 3A). A dictyosomal Golgi apparatus is located in the anterior end of the cell (Figs 2B, 2C, 3C, 3F). The cell also contains one or more series of flattened vesicles of consistent thickness, typically occurring in stacks of 3–4 units. These stacked-membrane structures (SM) appear in various places in the cell, and are clearly distinct from the Golgi apparatus (Figs 2C, 3C). Their membranes are more densely staining than those of the Golgi vesicles, and they contain material that is finely granular, but not very electron-dense (Fig. 3C, D). The material in the lumen of most SM units is about 60 nm thick, but in some individual units can be half as thick, usually changing within the same unit abruptly to full width (data not shown). In many cells, a large vesicle connects to the posterior flagellar pockets to form a pouch-like extension (Fig. 3B). The connection is at the base of the flagellar pocket, between the microtubular structures L2 and PS (see below). These vesicles, and occasionally the flagellar pockets, are filled with small (<100 nm across) nodules. These nodules frequently appear to be membrane-bound (Fig. 3A–D), and they probably represent remnants of extrusome material (see below). Food vacuoles are found throughout the cell, although more often in the ventral and posterior regions (Fig. 2A–C). Some sections also include non-membrane-bound electron-lucent spherical regions of 200-300 nm diameter, which might represent the remains of lipid droplets (Figs 2D, 3D).

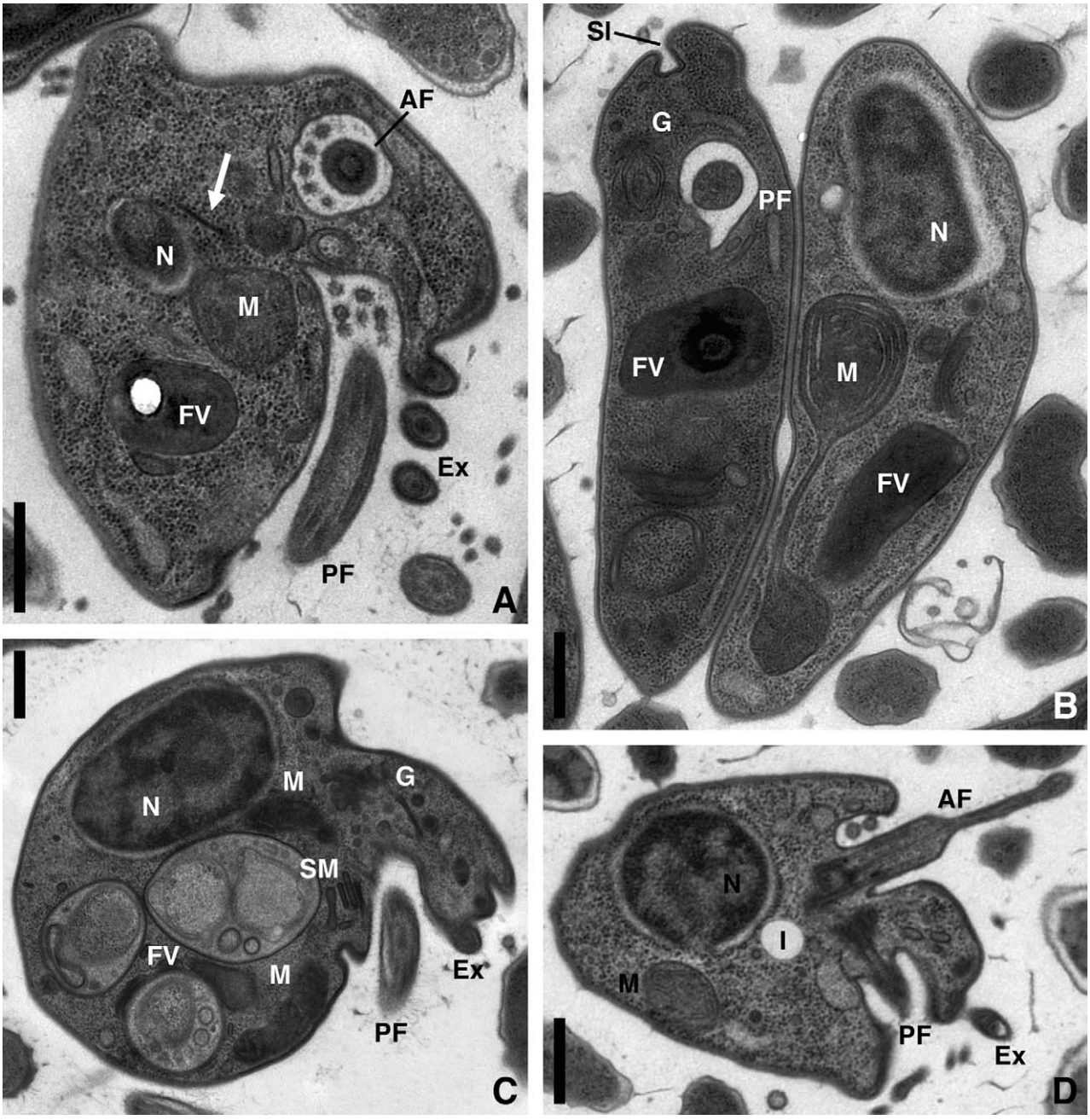

Figure 2. Transmission electron micrographs of whole cells. **A:** Section perpendicular to anterior flagellum, showing anterior portion of cell. Dorsal is to the left. The location of the rostrum is denoted by the extrusomes (Ex). Note extension of posterior flagellar pocket membrane into main body of cell (arrow). **B:** Section through narrower aspect of two cells. Left cell is sectioned perpendicularly to posterior flagellum. **C:** Oblique section through cell. Anterior flagellum emerges near concavity at upper right. Dorsal is to the upper left. **D:** Both basal bodies, showing orientation of both flagella and extent of flagellar pockets. This cell was one of a pair in late stages of cytokinesis (it is the same cell shown in Fig. 7E, F), although the configuration of its flagellar apparatus did not differ from that of interphase cells.Section thickness: A, D: 50 nm; B, C: 70 nm. A is tilted 30°; all others are untilted. Scale bars: 0.5 μm in each image. Abbreviations: [AF]: anterior flagellum; [Ex]: extrusome; [FV]: food vacuole; [G]: Golgi apparatus; [I]: electron-lucent inclusion; [M]: mitochondrion; [N]: nucleus; [PF]: posterior flagellum; [SM]: stacked membranes, [SI]: anterior slit.

There are generally seven extrusomes in the rostrum. These are arrayed in a staggered double row, with four on the margin of the posterior channel and three leftwards and dorsal to that (Fig. 3E, F). The extrusomes have a bulbous base about 90–100 nm in diameter, and a conical tip about 100 nm long. The tip has a complex substructure, including a relatively electron-dense cap (Fig. 3F, G). Each extrusome is bounded by a single membrane (Fig. 3G). Rounded vesicles about 90-100 nm across with structured contents, representing undocked extrusomes, may be seen in the cytoplasm near the rostrum (Fig. 3F). In other parts of the cell, larger vesicles with more homogeneous contents are frequently observed (e.g. arrowheads in Fig. 3A, D). Most or perhaps all of these represent earlier developmental stages of the extrusomes. The discharges of the extrusomes are strands with bulbous ends. These strands have electron-dense centres surrounded by a bilayer, and more electron-lucent material covering that (Fig. 3H). They are widespread throughout the intercellular medium (e.g. Fig. 2A, D), suggesting that many discharged just prior to or during the fixation process.

A distinct pellicle underlies the plasma membrane (the use of the term 'pellicle' for this structure follows other recent studies of *Ancyromonas* and apusomonads – see Cavalier-Smith and Chao 2010; Cavalier-Smith et al. 2008). This consists of a single undifferentiated sheet of electron-dense material, generally as thick as the lipid bilayer and mostly adpressed to it (Fig. 3I, J). The pellicle is absent at the base of each flagellar pocket as well as from the channel. Under favourable conditions the electron-dense sheet can be seen to be subtended by a thicker layer with little electron density (Fig. 3H, I). This subtending electron-lucent material is thickest and most conspicuous at the edges of the pellicle (Fig. 3J). A glycocalyx of consistent thickness (approx. 30 nm) surrounds the entire plasma membrane (Fig. 3H–J). In many sections this appears to have a very thin and somewhat electron-dense outer layer (Fig. 3I).

Flagellar Apparatus

Both flagella have a largely conventional structure (Figs 3E, 4G). The central pair of the axoneme persists through the acroneme, when present, of at least the anterior flagellum (Fig. 2D). The transition zone of the anterior flagellum contains a conspicuous electron-dense ring within the axoneme (Fig. 4A, F). A more-diffuse region is present in the posterior flagellum (Figs 3E, 5E). In both flagella the central pair originates at an electron-dense, spool-shaped axosome, located slightly below the level of insertion, which we treat as defining the distal end of the basal body (Figs 4A, 4B, 5C). Basal body substructure is difficult to resolve due to the extensive densely staining material encompassing the microtubules (Figs 4G, 5B, 6A). Basal bodies have at most a very indistinct cartwheel structure near their base, which is more usually observed in newly-forming basal bodies (Fig. 7A, B). The proximal ends of both basal bodies appear 'bevelled' (sensu Brugerolle 2002) rather than perpendicular to their axis (Figs 2D, 3E, 4A). The fully cylindrical portions of the basal bodies are about 250 nm long. A single electron-dense fibre with faint longitudinal striations connects the two basal bodies across their dorsal surfaces (Fig. 4G).

The flagellar apparatus associated with the anterior basal body consists of one pair of slightly separated microtubules (the anterior root), and another singlet microtubule (the anterior singlet). The anterior root originates near the left-posterior edge of the anterior basal body, between it and the posterior basal body (double arrow in Fig. 4B, C, E–G; see also Fig. 5B). It runs parallel to the anterior basal body along the left wall of the anterior flagellar pocket (double arrow in Fig. 4E, F). It then deflects to the left and continues along the cell periphery, supporting the dorsal lip of the anterior slit, and ultimately curving back to the posterior to support the margin of the rostrum (Fig. 5G). We did not determine its point of termination. The anterior singlet originates near the anterior-right edge of the anterior basal body (single arrow in Fig. 4B, C). It runs parallel to the right side of the basal body (single arrow in Fig. 4E–H), directly opposite to the anterior root. The anterior singlet is straight and very short, terminating near the opening of the flagellar pocket. Although most sections show a single microtubule, the anterior singlet may actually contain two microtubules for a short distance (probably less than 100 nm) shortly after its origin (not shown). As they extend along the walls of the flagellar pocket, both the anterior root and the anterior singlet pass into a ring of diffuse dense material that supports the edge of the pellicle where it ends midway down the flagellar pocket (Fig. 4A, E).

There are two distinct multi-microtubular roots associated with the posterior basal body, and one singlet root. One multi-microtubular root is closely associated with the right/posterior side of the basal body. Close to its origin, this root appears in cross section as a semicircular crescent of eight microtubules supported on the concave ventral side by a narrow transverse band of electron-dense mate-

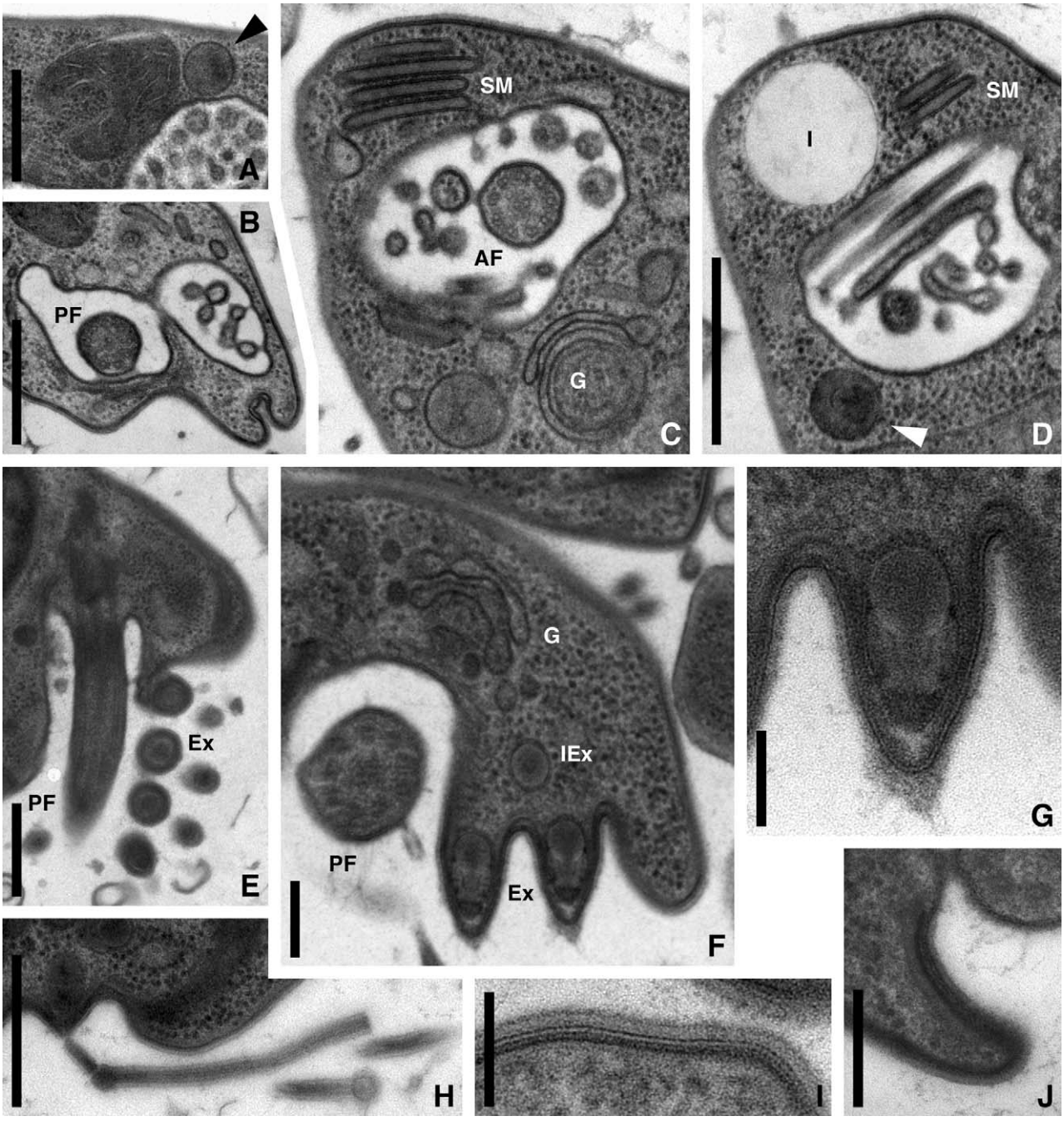

Figure 3. Transmission electron micrographs of subcellular features. **A:** Mitochondrion, showing both irregularly located flat cristae and cup-shaped configuration of organelle. Also visible is a probable immature extrusome (arrowhead, upper right) and the contents of a flagellar pouch (bottom right). **B:** Posterior flagellar pocket and adjoining pouch. **C, D:** Non-consecutive sections through anterior of cell, showing Golgi apparatus and separate stacked membranes in C, electron-lucent inclusion (probable lipid droplet) and immature extrusome (arrowhead) in D, and enlarged anterior flagellar pocket with membrane-bound material in both. **E:** Cross-section of extrusomes and longitudinal section of posterior flagellum. **F:** Golgi apparatus, immature extrusome, and longitudinal section through both rows of mature extrusomes within the rostrum. **G:** Closeup of right extrusome in F. **H:** Extrusome discharge. Extrusome apparently in the act of discharge is visible in the left of the micrograph. **I:** Plasma membrane of dorsum of cell, with dense and lucent layers of pellicle beneath and glycocalyx above it. **J:** Edge of flagellar pocket, showing fine structure of pellicle, with thickened subpellicular layer. Section thickness:

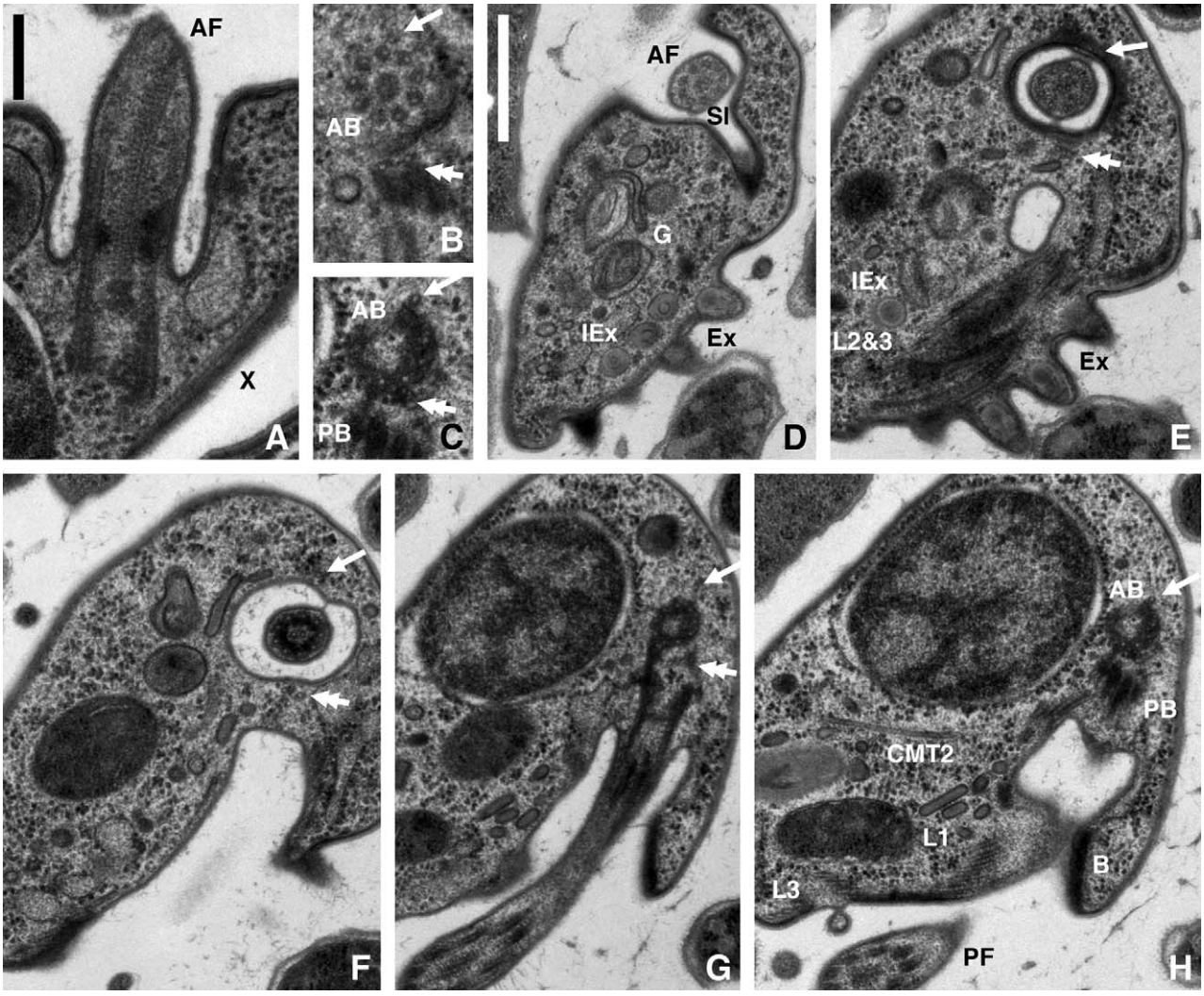

Figure 4. Transmission electron micrographs aligned through anterior basal body, showing anterior root (AR, double-headed arrow) and anterior singlet root (AS, single-headed arrow). **A:** Longitudinal section of anterior flagellum, as well as peripheral microtubule group X. **B:** Transverse section of axosome and both anterior roots. **C:** Proximal end of basal body, near origins of both anterior roots. **D–H:** Non-consecutive series through anterior flagellum and basal body (C is a close-up of H). Besides anterior roots, note anterior slit and collection of immature extrusomes in D, longitudinal section of superimposed posterior roots in E, longitudinal section through proximal portion of posterior flagellum in G, and longitudinal sections of posterior roots as well as cross-section of dense bridging material in H. All sections are 50 nm thick. B is tilted at 30°; all others are untilted. Scale bars: 0.2 μm (A–C); 0.5 μm (D–H). Abbreviations: [AB]: anterior basal body; [AF]: anterior flagellum; [B]: bridging material of posterior flagellar pocket; [CMT2]: microtubule 2 from crescent root system; [Ex]: extrusomes; [G]: Golgi apparatus; [IEx]: immature extrusomes; [L1]: posterior root L1; [L2&3]: posterior root elements L2 and L3; [SI]: anterior slit; [X]: peripheral microtubule group X.

A, E–G, I: 70 nm; B–D, H, J: 50 nm. Tilt angles: B: 20°; C, D: 35°; H: 30°; all others are untilted. Scale bars: 0.5 μm (A–E, H); 0.2 μm (F); 0.1 μm (G, J); 50 nm (I). Abbreviations: [AF]: anterior flagellum; [Ex]: extrusome; [G]: Golgi apparatus; [I]: electron-lucent inclusion; [IEx]: immature extrusome; [PF]: posterior flagellum; [SM]: stacked membranes.

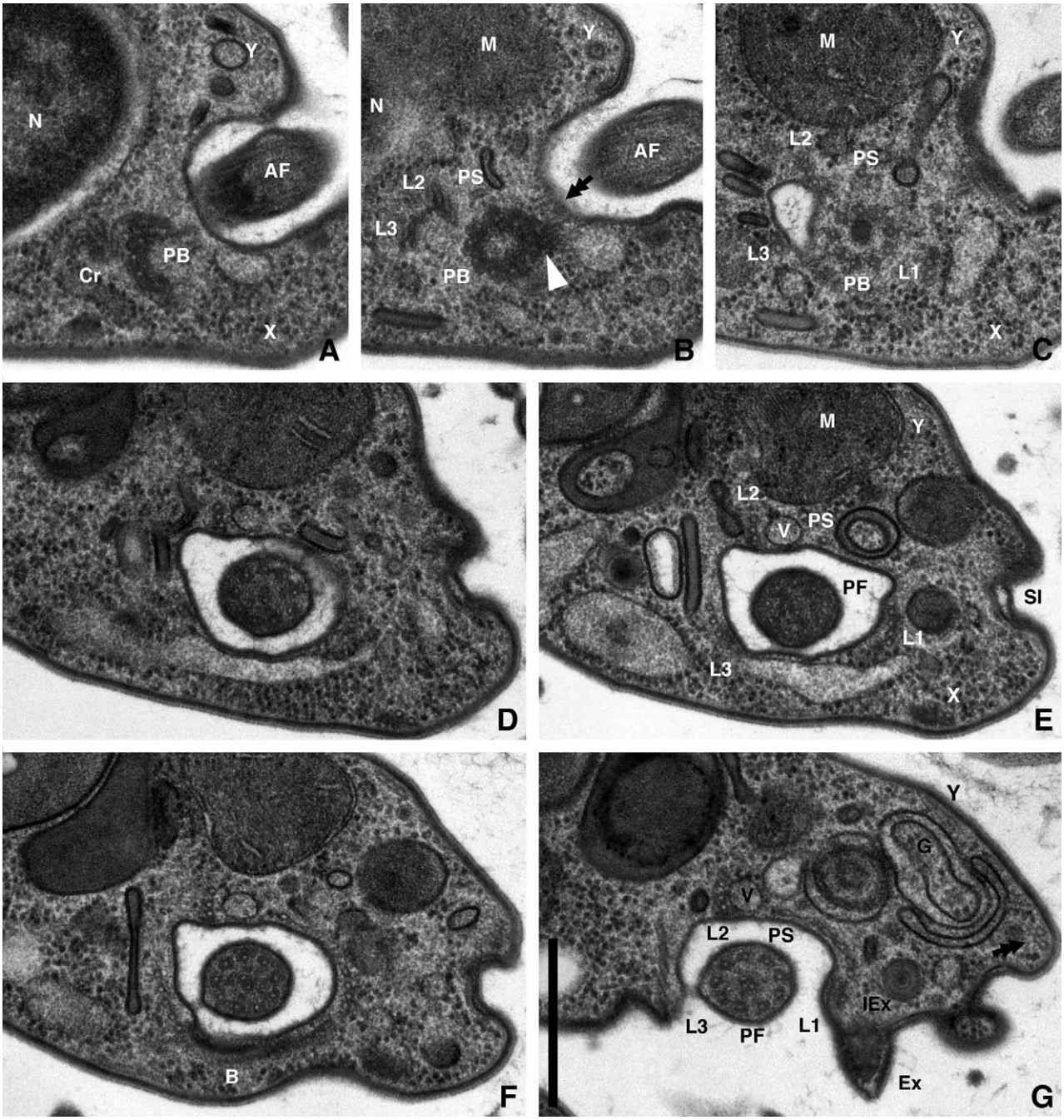

Figure 5. Non-consecutive series of transmission electron micrographs aligned to posterior basal body. **A:** Proximal end of posterior basal body, with L2 and L3 adjoining to form (most of) the crescent structure. Peripheral microtubular groups X and Y are both visible (the former sectioned obliquely). **B:** Distal to where the crescent structure disappears, L2 and L3 splay out from the crescent structure, while L1 originates linked to the posterior basal body by the spur (arrowhead), and the posterior singlet PS can be seen slightly distal to its origin, near L2. L2 still has four microtubules. The anterior root (double arrow) can also be seen between the flagella/basal bodies. **C:** The base of the posterior flagellar pocket begins to form at the level of the axosome, separating L2 from L3. L2 has four microtubules (one indistinct in this micrograph). At this level L3 still has only two microtubules, while L1 has three. **D:** Distal to the point of flagellar separation, the cylindrical vesicle lies between L2 and PS. L3 still has only two microtubules. **E, F:** Approaching the opening of the flagellar pocket, L1 and L3 each acquire more microtubules, while 'X' terminates near L1, and the bridging material across the dorsal

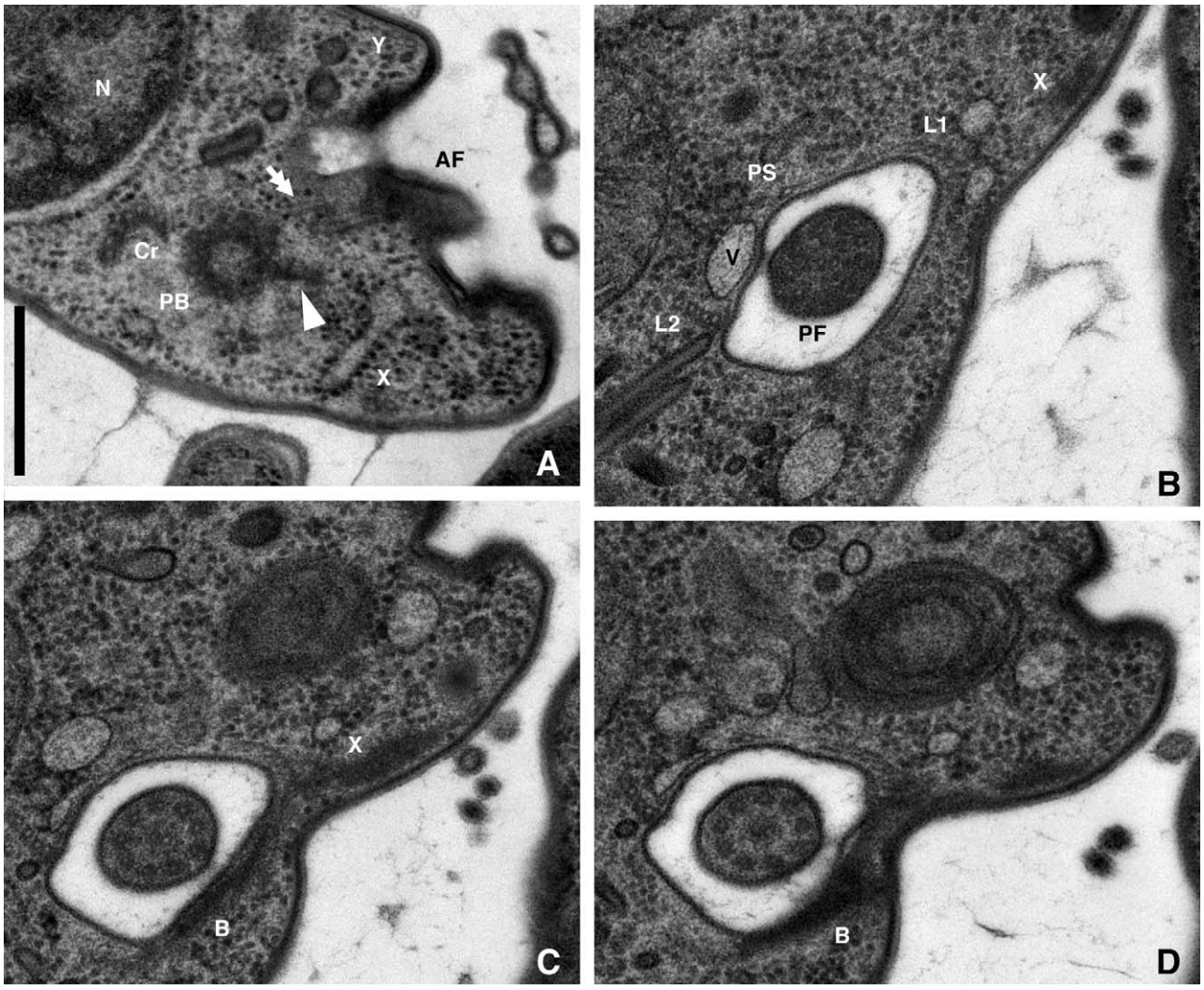

Figure 6. Transmission electron micrographs of additional sections aligned to posterior basal body. **A:** Crescent structure (Cr), and the spur associated with the origin of L1 (arrowhead). Note also the anterior root (double arrow). **B–D:** Non-consecutive sections (exactly one section in between adjacent figures) of the distal portion of the flagellar pocket, showing termination of peripheral microtubule group X and associated dense material, which appears continuous with the bridging dense material bordering the ventral face of the posterior flagellar pocket. All sections are 50 nm thick. A is tilted at 20°; others are not tilted. Scale bar: 0.5 μm. Abbreviations: [AF]: anterior flagellum; [B]: bridging dense material; [Cr]: crescent structure; [L1]: posterior root L1; [L2]: posterior root element L2; [PB]: posterior basal body; [PF]: posterior flagellum; [PS]: posterior singlet root; [V]: vesicle associated with posterior flagellum; [X]: peripheral microtubule group X; [Y]: peripheral microtubule group Y.

face of the flagellar pocket appears (B in Figure 5F). **G:** The posterior flagellar pocket has opened up into the posterior channel, bordered on the lateral side by the rostrum with its extrusomes. L1 and L3 each comprise five microtubules, although these begin to angle away from perpendicularity to the plane of section. PS is linked to L1 by a delicate connection. Note the anterior root (double arrow) supporting first the dorsal margin of the slit, then the outer margin of the rostrum. All sections are 50 nm thick, tilted at 10°. Scale bar: 0.5 μm. Abbreviations: [AF]: anterior flagellum; [B]: bridging material; [Cr]: crescent structure; [Ex]: extrusome; [G]: Golgi apparatus; [IEx]: immature extrusome; [L1]: posterior root L1; [L2]: posterior root element L2; [L3]: posterior root element L3; [M]: mitochondrion; [N]: nucleus; [PB]: posterior basal body; [PF]: posterior flagellum; [PS]: singlet posterior root; [SI]: anterior slit; [V]: vesicle associated with posterior flagellum; [X]: peripheral microtubule group X; [Y]: peripheral microtubule group Y.

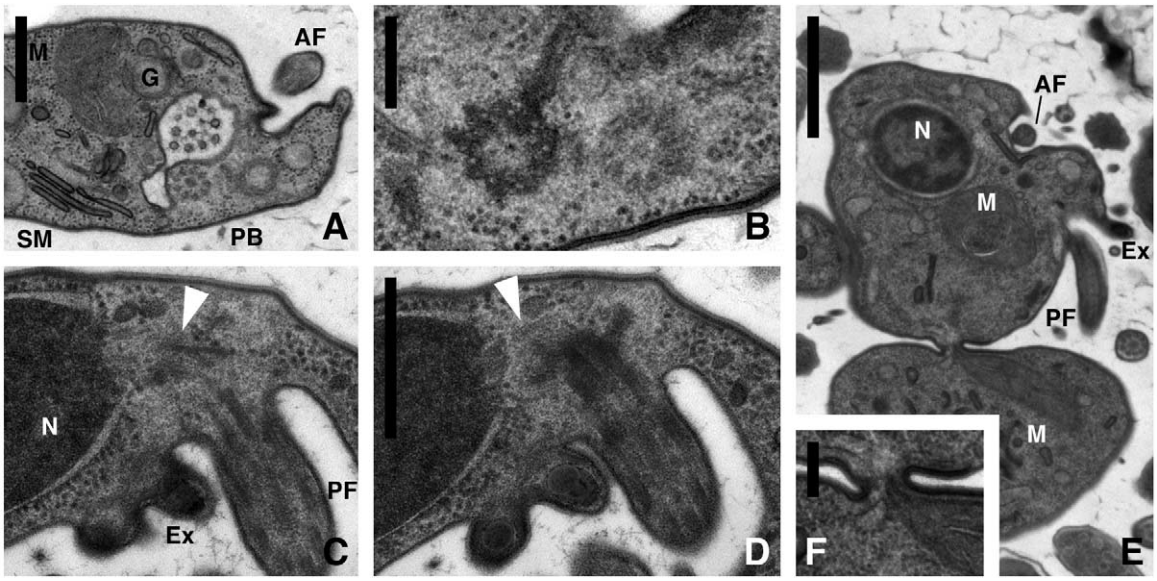

Figure 7. Transmission electron micrographs of cells in varying stages of division. **A, B:** Non-consecutive series from premitotic cell showing replicating posterior basal bodies. **C, D:** Consecutive sections from a cell in late-stage mitosis, showing microtubules protruding through an enlarged opening in the nuclear envelope to join to the posterior basal body (arrowheads). **E:** Cells in the last stages of cytokinesis, with only a narrow bridge connecting the two. **F:** Closeup of E, showing the bridge close to one margin of the pellicle (right), and the 'shared' mitochondrion. All sections are of 50 nm thickness and are untilted. Scale bars: 0.5 μm (A; C–D); 0.2 μm (B); 1.0 μm (E); 0.1 μm (F). Abbreviations: [AF]: anterior flagellum; [Ex]: extrusome; [G]: Golgi apparatus; [M]: mitochondrion; [N]: nucleus; [PB]: posterior basal body; [PF]: posterior flagellum; [SM]: stacked membranes.

rial ('Cr' in Fig. 6A). The microtubules comprising this structure splay out within 50 nm of either side of the electron-dense material (Fig. 5A, B); on the proximal side they project toward the base of the anterior basal body (particularly the rightmost two, which correspond to L3 – see below). On the distal side, the microtubules separate into four groups. Two of these correspond to the multi-microtubular elements called L2 and L3 by Mylnikov (1990); we retain these designations. L3 initially consists of the two posterior/rightmost microtubules (i.e. furthest from the basal body) in the crescent structure (Fig. 5B, C). It runs along the posterior/right side of the flagellar pocket (Fig. 5C–G). At about the level of flagellar emergence, L3 begins to acquire additional microtubules, added one at a time to the ventral side of the root, reaching a maximum of five (Fig. 5E, F). L2 initially comprises the four crescent microtubules closest to the basal body (Fig. 5A–C). One microtubule in this element (the one closest to the centre of the crescent) appears to terminate at around the level of the axosome (Fig. 5C, D); the remaining three microtubules persist for the remainder of the root (Fig. 5D–G). L2 runs along the dorsal side of the flagellar pocket, but perpendicular to the flagellar pocket membrane. In between L2 and L3 in the crescent are two individual microtubules: right to left these are crescent microtubules 1 and 2 (CMT1 and CMT2). These two microtubules diverge very close to the crescent structure, both from the multi-microtubular components and from each other. Each deflects rightward: CMT1 associates with the anterior mitochondrion, while CMT2 roughly follows the nuclear surface, albeit at a distance (e.g. CMT2 in Fig. 4H).

The two other roots, the L1 of Mylnikov (1990) and the posterior singlet, have independent origins from the crescent structure. L1 originates on the left-anterior side of the posterior basal body. Near its origin it is associated with a spur of electron-dense material that projects from the proximal end of the posterior basal body (arrowhead in Fig. 5B). It runs along first the left side of the flagellar pocket and then the channel, directly opposite to L3 (Fig. 5C–G). Much like L3, L1 has two microtubules, to which are added more, one by one, starting at around the level of the transition zone, to a maximum of five, which is reached at around the opening of the flagellar pocket (Fig. 5G). Unlike L3, these additional microtubules are added to the dorsal side of the root. The posterior singlet originates near the dorsal-right side of the

posterior basal body, close to the crescent structure (Fig. 5B). It runs along the dorsal side of the posterior flagellar pocket, to the left of L2 (Fig. 5C–G).

The posterior flagellar pocket and channel thus have a characteristic appearance in transverse section (Fig. 5F, G). They are framed on either side by L3 and L1, with L2 and the posterior singlet lining the dorsal side, nearest the anterior flagellum. Between the posterior singlet and L2 lies a cylindrical endomembrane vesicle, whose axis runs parallel to all posterior flagellar roots (Fig. 5D–G), and which we did not find to have any obvious connection with other cell compartments or cytoskeletal elements. Towards the opening of the pocket, the microtubules in L3, and especially those of L1, splay out a little from one another, but remain joined by fine connecting material (Fig. 5F, G). A similar connection also continues dorsally from L1 to attach to the posterior singlet. Near the opening of the pocket, L1 and L3 are themselves connected by their ventral edges, by a complex of electron-dense material that underlies the membrane along the ventral side of the posterior flagellar pocket (Figs 5F, 6B–D). This structure continues for about 200–300 nm (Fig. 4G, H), forming the support of the margin of the pocket as it opens ventrally into the channel that separates the rostrum from the main cell body (Fig. 6C, D). This material also connects to the pellicle, and to the electron-dense material associated with peripheral microtubular group X (see below), although the pellicle is more sharply defined than these other electron-dense elements (Fig. 6C, D).

L1, L2, L3, and the posterior singlet all persist along the channel demarcating the edge of the rostrum (Fig. 8A). Towards the end of the rostrum, these various elements approach one another (Fig. 4E). L2 runs immediately to the right of L3, and both run in a plane parallel to but positioned more dorsally than L1 (Fig. 4E, H), although L3 then curves dorsally to pass through the plane of L1 (Fig. 4H). The posterior singlet diverges from L1–3, ultimately running to their anterior/right.

We also identified three groups of peripheral microtubules, ‘X’, ‘Y’ and ‘Z’, which all appeared consistently in several examined cells. Group X is a doublet that is first observed on the right side of the cell, between the nucleus and pellicle. It runs anteriorly-leftwards, passing close to the proximal end of the anterior basal body (Fig. 4A). It then runs first anterior-leftwards (roughly parallel although not close to the anterior flagellum), and then posterior-dorsally, up to the ventral side of the base of the rostrum (Figs 5A–E, 6A). There X becomes associated with a thick electron-dense element (Fig. 5D, E). Its component microtubules terminate in the vicinity of the opening of the posterior flagellar pocket, at least one abutting or approaching L1 (Fig. 6B–D). Group Y is usually observed as a triplet, and runs from within the rostrum near the anterior root, across the anterior face of the cell and dorsal to the anterior flagellar pocket, to curve between the nucleus and the pellicle on the right side of the cell (Figs 5A–G, 6A, 8B, 8C). Group Z is an array of at least three more-widely-spaced microtubules. It runs across the dorsum, from the anterior root in the rostrum (possibly close to group Y) across to the right (Fig. 8B, C). We have no indication of polarity for the microtubules in any of these groups: while one end of each is associated with a flagellar root (L1 for group X, and AR for groups Y and Z), the location of the other end is unknown. We also identified a small number of single peripheral microtubules within the rostrum and along the ventral side of the cell, but did not trace their paths extensively and did not include them in our reconstruction.Reconstructions of the cytoskeleton are shown in Figs 8 and 9.

Division

A few cells were fixed during cell division (Fig. 7). Basal bodies are replicated before mitosis begins (Fig. 7A, B). Mitosis appears to be semi-open, as cells in the later stages of cytokinesis have microtubules that originate from around the basal bodies and extend into the interior of daughter nuclei through a large opening in the otherwise intact nuclear envelope (arrows in Fig. 7C, D). The position of the basal bodies is consistent with a biradial symmetry during cytokinesis, roughly in the transverse plane and perpendicular to both anterior basal bodies. Representing a later stage of division, we found two cells connected by a narrow bridge (Fig. 7E). The pellicle is prominent in the bridge between these two cells, and terminates nearby (Fig. 7F). A mitochondrion is shared between the two in the cells that we observed, presumably either in the process of transferring to one daughter cell only, or being divided between them (Fig. 7F).

Discussion

Comparison with Previous Accounts of *Ancyromonas*

Prior to this study, the most detailed ultrastructural work on *Ancyromonas sigmoides* was a

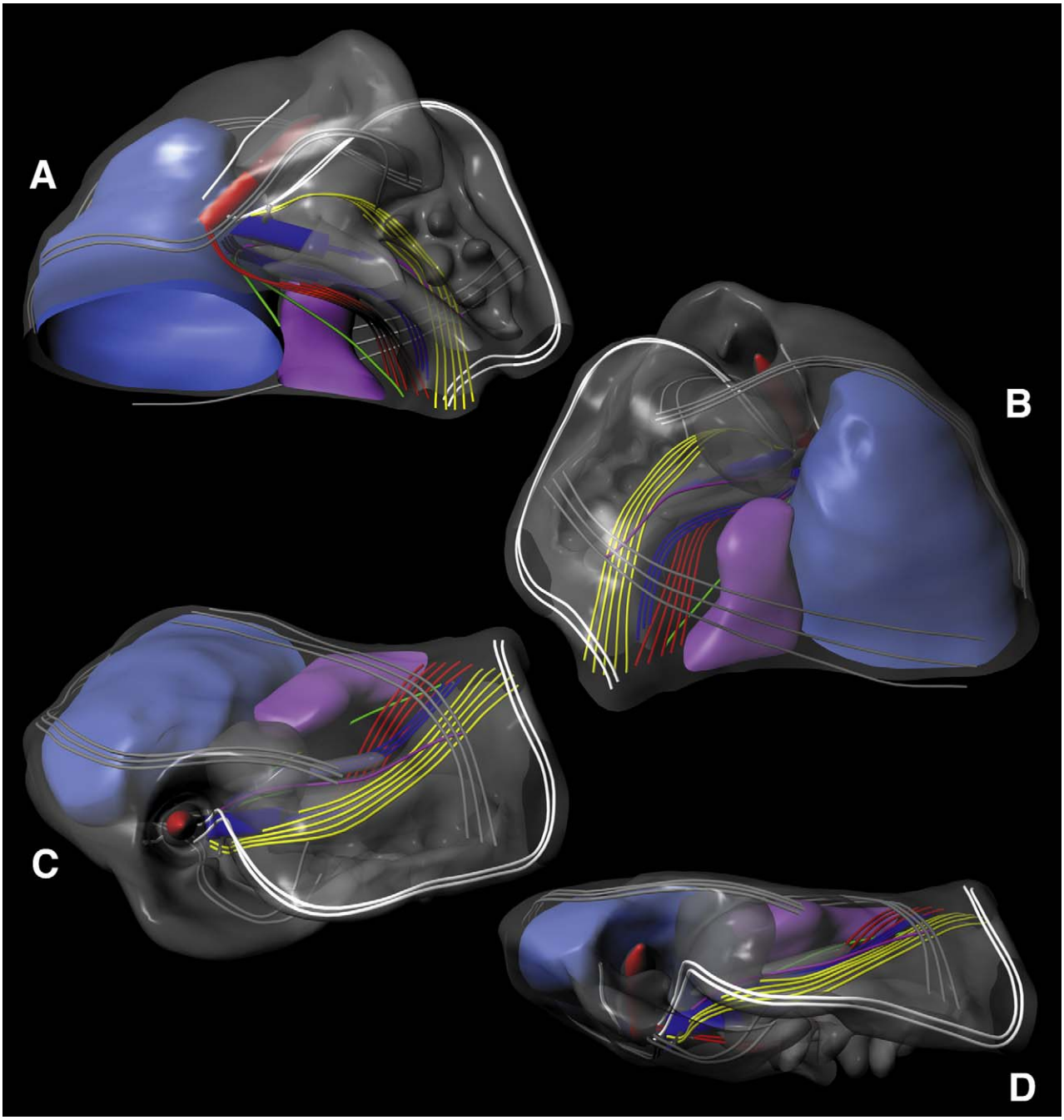

Figure 8. Three-dimensional reconstruction of the anterior portion of *Ancyromonas sigmoides*, based on annotated serial sections. In all images, the nucleus is blue and the mitochondrion purple; all other membranous structures are transparent grey, and proteinaceous structures are dark grey. Microtubular structures are coloured as indicated in Figure 9. **A:** Ventral aspect. **B:** Dorsal aspect. **C:** Aligned with anterior flagellum. **D:** Anterior aspect. Note that Figures 8A and 9A are in the same orientation.

general survey by Mylnikov (1990). Additionally, Cavalier-Smith et al. (2008) reported some TEM data from *Ancyromonas micra* (= *Planomonas micra*). Our general observations (exclusive of the microtubular cytoskeleton: see below) are mostly consistent with these previous reports. Some differences are likely a consequence of our use of freeze-substitution. We were also examining serial sections, and, likely, a greater quantity of raw data.

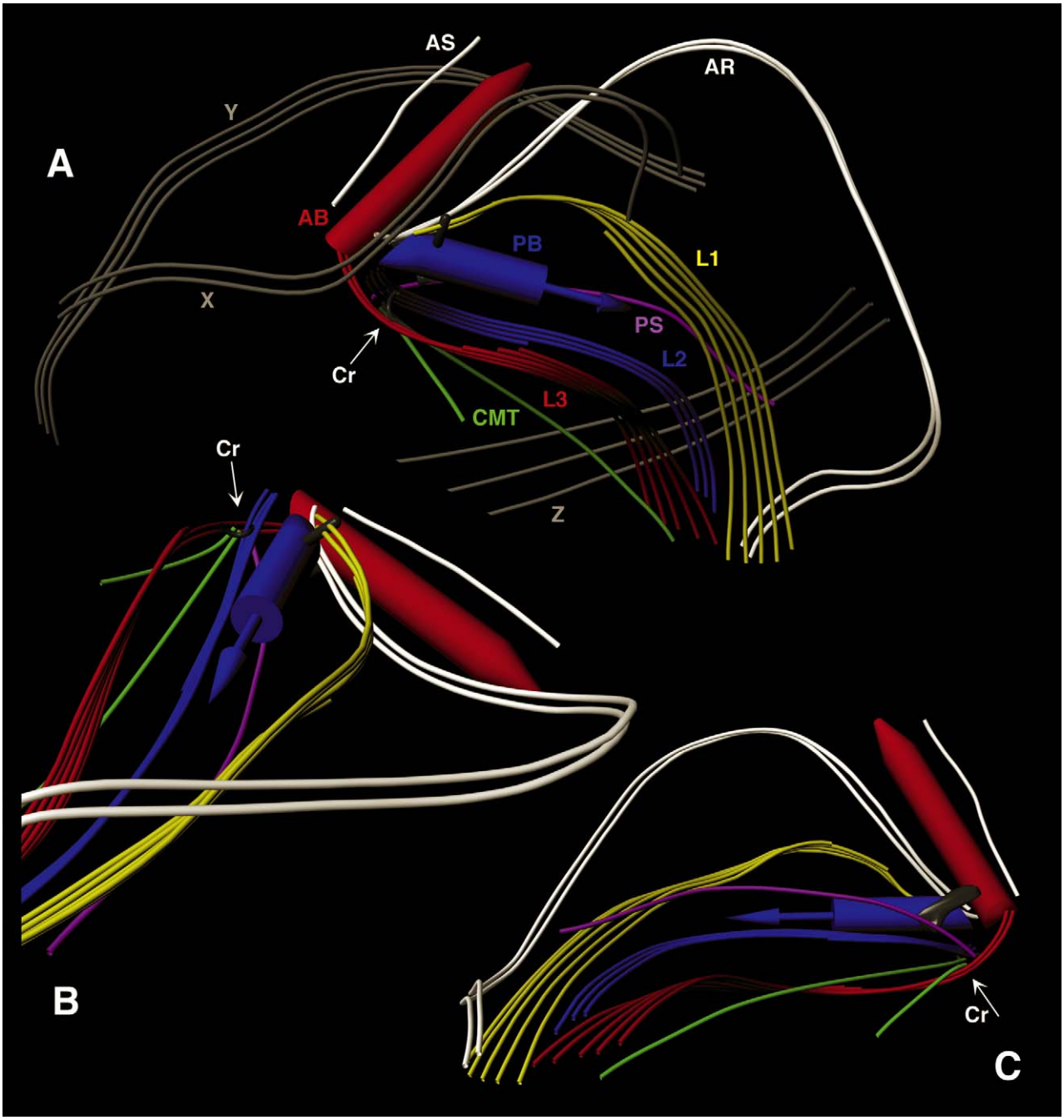

Figure 9. Three-dimensional reconstruction of the flagellar apparatus of *Ancyromonas sigmoides*. All membranous structures have been removed from the model. Groups of peripheral microtubules are shown only in A. **A:** Ventral aspect, identical to that in Figure 8A. Note crescent structure (Cr). Peripheral microtubule group Y probably originates in the vicinity of AR (much as Z is shown here), but it was not possible to determine its precise origin from the series used for this model. **B:** Ventral-left aspect, showing crescent structure. **C:** Dorsal aspect, rotated with anterior away from viewer, Abbreviations: [AB]: anterior basal body; [AR]: anterior root; [AS]: anterior singlet; [CMT]: crescent microtubules; [Cr]: crescent structure; [L1]: posterior root L1; [L2]: posterior root element L2; [L3]: posterior root element L3; [PB]: posterior basal body; [X]: peripheral microtubule group X; [Y]: peripheral microtubule group Y; [Z]: peripheral microtubule group Z.

Mylnikov (1990) found homogeneously distributed chromatin in the nucleus, while we saw distinguishable euchromatin and heterochromatin. Mitochondrial cristae were quite variable in our preparation, ranging from loose sacs to disc-like compressed laminae to very large flat structures. This encompasses the previous observations of *A. sigmoides* (Mylnikov 1990) and of *A. micra* (Cavalier-Smith et al. 2008), although the cristae might be more consistently discoidal in the latter species. The electron-lucent inclusions that we alone observed may be lipid droplets whose contents leached out during fixation (a known phenomenon in freeze-substitution preparations: Hippe and Hermanns 1986; Lancelle et al. 1986). While our series did not encompass any cells in their entirety, we found that many cells have at least two separate mitochondria, rather than only one (Cavalier-Smith et al. 2008; Mylnikov 1990).

The stacked membrane structures we observed are also visible in Mylnikov's (1990) micrographs, although in his material the individual units appear more inflated than is typical in ours. The lumen material in our preparation is similar in electron density and appearance to the glycocalyx. The thickness of this material is almost always twice that of the glycocalyx, the exceptions being cases in which the luminal material is as thick as the glycocalyx. We suggest that the stacked-membrane organelles may function in the building or maintenance of at least some of the cell's surface structures.

Mylnikov (1990) linked the small dense spherical bodies with both the Golgi apparatus and the extrusomes. He considered them to be immature extrusomes, in transit from the Golgi apparatus to their functional position on the rostrum rim. Our observations are consistent with this. Cavalier-Smith et al. (2008) reported a single microbody placed immediately posterior to the nucleus, with an appearance much like these immature extrusomes, while we find several such bodies, and in various locations. This discrepancy could be due to fixation or species differences. It is also possible that Cavalier-Smith et al. (2008) observed a different organelle, unrelated to the extrusomes.

We found no evidence of pseudopodia in our material, and previous accounts of pseudopodia in *Ancyromonas* are dubious. According to Cavalier-Smith et al. (2008), Mylnikov (1990) stated that *Ancyromonas* "has extremely slender branching pseudopods". This appears to be an error: what Mylnikov (1990) actually labels as a pseudopodium is a broad, unbranched region, probably a flange of the cell body, and not a discrete structure. Cavalier-Smith et al. (2008) noted 'wispy material' near *A. micra* cells, and suggested that this represents either very fine filopodia, fixation artefacts, or secreted material. The latter two interpretations are the more credible.

One of the features proposed to unite *Ancyromonas* with apusomonads is the shared presence of a continuous electron-dense pellicle (Cavalier-Smith 2002, 2003, 2009; Cavalier-Smith et al. 2008). Our observations of the pellicle are consistent with previous accounts of a single dense layer. The subtending electron-lucent material beneath the electron-dense layer of the pellicle has not been noted previously, possibly due to fixation differences. Mylnikov (1990) previously drew attention to the glycocalyx, which we find to be of constant thickness, with a much thinner and somewhat denser bounding layer.

In the flagella themselves, we confirm Mylnikov's (1990) observation of dense material above the axosome. Cavalier-Smith et al.'s (2008) preparations of *Ancyromonas micra* do not have this, instead showing a moderately-staining cylinder in the anterior flagellum (Cavalier-Smith et al. 2008). Such a cylinder is present in our preparations as well, but is difficult to distinguish due to the electron-dense material. The lack of dense material in *A. micra* is either a species-level difference or one of fixation protocol. Cavalier-Smith et al. (2008) mention a dense amorphous plate below the axosome in their abstract, but do not elaborate on this in their results; we did not see such a structure.

The current study significantly clarifies and extends our understanding of the cytoskeleton of *Ancyromonas*. According to Cavalier-Smith et al. (2008), Mylnikov (1990) had reported three microtubular roots, one associated with the anterior basal body, and two with the posterior basal body. Mylnikov (1990) indeed reported three microtubular roots — L1, L2, and L3 — but he associated all of them with the posterior basal body. In practice, L2 and L3 appear to be two elements of a single microtubular complex, originating to the right of the posterior basal body, namely the crescent root. Apart from the details of its origin (see above), we find L2 largely as Mylnikov did, aside from its comprising three microtubules at minimum, as opposed to his two. Mylnikov (1990) reports six microtubules in L3, not five. By contrast to L2 and L3, we traced Mylnikov's L1 root to an origin near the left side of the posterior basal body. L1 has at most five microtubules, while Mylnikov (1990) again specifies up to six. In this case, it appears that he included the microtubule we identify as the posterior singlet as the sixth microtubule

in L1. The singlet does develop a thin connection to L1 similar to the connections between the microtubules within L1; however, the posterior singlet originates near the crescent structure, well separated from L1, and is clearly a distinct element. Mylnikov (1990) also observed a pair of microtubules close to the anterior flagellum. He associated these with L2, but they were probably the anterior root, which originates near the proximal end of L2. The other single microtubules (the anterior singlet, CMT1, and CMT2) were also overlooked previously. Previous accounts do not include any peripheral microtubules, although the peripheral elements that we did find each contained only a few microtubules, and would be easily overlooked.

We thus find that *Ancyromonas*'s flagellar apparatus is significantly more complex than had previously been reported. The additional components and relationships between components that were identified are important to consider in comparing *Ancyromonas* to other organisms.

Comparison with Apusomonads and some Other Proposed Apusozoa

The only apusomonad for which there are detailed cytoskeletal data published is *Apusomonas* itself (Karpov 2007). The anterior flagellar apparatus of *Apusomonas* appears more developed than that of *Ancyromonas*. *Apusomonas* has a broad 'right microtubular root' that lies to the right of the anterior basal body, a striated fibre running parallel to the broad root and in between it and the basal body, and a pair of dorsal microtubules running perpendicularly across the cell's dorsum from right to left (Karpov 2007). In contrast to the anterior roots of *Ancyromonas*, none of these run parallel to their associated basal body. However, the anterior root of *Ancyromonas*, while initially parallel, does turn off to the left of the basal body to support more-dorsal structures, much like the pair of dorsal microtubules in *Apusomonas*.

In its posterior flagellar apparatus, *Apusomonas* has a rhizostyle, which is a broad compound root comprising about ten microtubules with axial ridges and a dorsal sheet of nonmicrotubular material, and a doublet element that splits off from the rhizostyle shortly after its origin (Karpov 2007). The rhizostyle complex of *Apusomonas* is similar to the crescent root complex of *Ancyromonas* (including L2 and L3) in its position (to the right of the posterior basal body), in its splitting soon after its origin, and in the axial filaments along its individual microtubules, which have a parallel in the connections between the microtubules of L3 in *Ancyromonas*. However, the non-microtubular sheet on the dorsal surface of the *Apusomonas* rhizostyle has no obvious counterpart in *Ancyromonas*, the non-microtubular material in *Ancyromonas*'s crescent root being on the opposite (ventral) side of the root. The posterior flagellar apparatus of *Apusomonas* also has three other microtubules, which travel in parallel to the rhizostyle-derived doublet. Karpov (2007) referred to these three collectively as singlets, but also noted that they are not all of the same origin. Two of them are relatively closely associated with one another and originate on the dorsal/left side of the posterior basal body, more or less opposite to the rhizostyle. In contrast, the third appears to originate in the cytoplasm slightly dorsal to the posterior basal body, but linked to the rhizostyle by fine material (fig. 18 in Karpov 2007). If we regard the three 'singlet' microtubules as comprising two roots, a doublet and a singlet, they would occupy positions relative to the posterior basal body similar to L1 and the posterior singlet in *Ancyromonas*, respectively. Furthermore, the linkage between the singlet and the rhizostyle in *Apusomonas* is comparable to the linkage between the posterior singlet and L3 in *Ancyromonas*.

An intra-axonemal cylinder is located below the transition zone in *Apusomonas* (Karpov 2007), which has been compared with the cylinder found above the transition zone in *Ancyromonas* (Cavalier-Smith et al. 2008). Homology between the two is questionable because of this positional discrepancy. Further, the intra-axonemal cylinder is thin and sharply defined in *Apusomonas*, unlike the thicker, more amorphous material in *Ancyromonas sigmoides*. The basal bodies of *Apusomonas* are closer to the eukaryotic norm than those of *Ancyromonas*, with conspicuous cartwheel structures (Karpov 2007) and less pronounced 'bevelling'.

The flagella are oriented almost antiparallel to one another in *Apusomonas*, while they lie at close to a right angle apart in *Ancyromonas*. The basal bodies in *Apusomonas* are connected by two prominent fibrillar elements, one described as a 'wheel' between flanges of the proximal ends of the basal bodies (the 'fused feet'), and the other a complex multilayered fibrillar structure (MFS). The MFS in *Apusomonas* does not have a counterpart in *Ancyromonas*. The 'fused feet' in *Apusomonas* bear some resemblance to the connecting fibre in *Ancyromonas*, inasmuch as both are electron-dense structures with longitudinal striations, although with differing points of attachment as demanded by the differing geometry between the basal bodies.

Several apusomonad strains, formerly assigned to *Amastigomonas*, have been examined by TEM,

but none to the same level of detail as *Apusomonas proboscidea* (see Cavalier-Smith and Chao 2010 for an updated taxonomy of apusomonads). From the incomplete data available, their flagellar apparatuses appear similar to that of *Apusomonas* (Karpov 2007; Karpov and Mylnikov 1989; Molina and Nerad 1991), with only minor differences. One such difference is the presence in several strains of a posterior 'left root' or 'left band' of 3–5 microtubules, which lines the cell membrane alongside the usual location of the posterior flagellum. This is difficult to compare at present, because it is positionally similar to microtubules in *Apusomonas* that have several separate origins (the split element of the rhizostyle, and three other microtubules: see above and Karpov 2007). Equivalents of the MFS and transversely-oriented dorsal root of *Apusomonas* have not been observed yet in other apusomonads. The striated fibre is also known only in *Apusomonas* (Karpov 2007). This suggests that the striated fibre may be a derived trait for a relatively small subclade within apusomonads.

At this stage we cannot be confident that the similarities between *Ancyromonas* and *Apusomonas* extend to all apusomonads. More detailed study of more apusomonads is needed to clarify the characteristics of the group as a whole.

Another taxon conjectured to be related specifically to *Ancyromonas* is *Micronuclearia* (Cavalier-Smith 2009; Cavalier-Smith et al. 2008; Mikrjukov and Mylnikov 2001). *Micronuclearia podoventralis* is a non-flagellated amoeba, so its cytoskeleton offers little by way of points of comparison to *Ancyromonas*. As noted by Cavalier-Smith et al. (2008), *Micronuclearia*'s pellicle resembles that of *Ancyromonas* in having a single electron-dense layer underlying, and roughly the same thickness as, the plasma membrane (Mikrjukov and Mylnikov 2001). However, the pellicle in *Micronuclearia* is less closely adpressed to the membrane than in *Ancyromonas* (barring the latter's anterior slit), and micrographs of *Micronuclearia* do not show less electron-dense subtending material, although this could be a fixation difference. More detailed comparative data would be valuable.

Another enigmatic taxon previously suggested to be related to both *Ancyromonas* and the apusomonads is Hemimastigophora, mainly because its members have a dense pellicle (Cavalier-Smith 2003; Karpov 1990). The hemimastigophoran pellicle is similar in substructure to that of *Ancyromonas*, as visualised in the current study, in that it comprises a single electron-dense layer subtended by a thicker layer of electron-lucent material, each of comparable thicknesses to their counterparts in *Ancyromonas* (Foissner and Foissner 1993; Foissner et al. 1988). Differences in pellicle distribution in Hemimastigophora and *Ancyromonas* are discussed by Cavalier-Smith et al. (2008). The flagellar apparatus of hemimastigophorans comprises one long and one short root per flagellum. These each comprise two to four microtubules, run perpendicularly to their associated flagella, and serve to connect the flagella into kineties. This arrangement bears no special similarity to *Ancyromonas*. The flagella differ from those of *Ancyromonas sigmoides* in having shorter basal bodies with visible cartwheels nonetheless, no axosome, and a thin, well-defined transitional plate that reaches to the flagellar membrane. There is a thin cylinder within the transition zone in *Hemimastix*, as in *Ancyromonas micra* (Cavalier-Smith et al. 2008), although this appears to be larger in diameter, thinner-walled, and to have more conspicuous connections to the axonemal doublets. Overall, our observations only very marginally strengthen the very limited case for a relationship between Hemimastigophora and *Ancyromonas* and/or apusomonads.

Comparison with Excavates (and Other Taxa)

A possible phylogenetic link has been proposed between Apusozoa and Excavata based on the fact that both taxa bear grooves or channels used in feeding, and on their frequent placements in basal locations in molecular phylogenies of eukaryotes (Cavalier-Smith 2003). Further, recent multigene phylogenies place Excavata between 'unikonts' and other well-studied 'bikonts' in an unrooted tree (Burki et al. 2008; Hampl et al. 2009), which is within the range of phylogenetic positions that have been suggested for Apusozoa (Kim et al. 2006).

Excavate ultrastructure is well-characterised (Simpson 2003): 'typical excavates' have a ventral suspension-feeding groove, supported primarily by two multi-microtubular roots, positioned to the left and right, that are associated with the posterior basal body. The right root splits into two soon after its origin. A singlet root is also associated with the posterior basal body, and runs along the groove between the left root and inner right root. There are also usually three conspicuous nonmicrotubular fibres ('I', 'B', and 'C').

We find similarities to several of these features in *Ancyromonas sigmoides*. The crescent root of *Ancyromonas* occupies a similar place to the right root of excavates relative to the posterior basal body and the channel. Like the right root of excavates,

the crescent root of *A. sigmoides* also splits (into L2 and L3). The non-microtubular component of the crescent structure itself occupies a place similar to the I fibre in excavates (on the ventral side of the microtubular ribbon), although the crescent structure is far smaller and has no particular similarity in substructure. The presence and position of the posterior singlet in *A. sigmoides* corresponds well to that of the singlet root in typical excavates. Some excavates have a vesicle of rough endoplasmic reticulum adpressed to the dorsal face of the inner right root, that is, the side facing the singlet root (Simpson and Patterson 1999, 2001). This is essentially the same position as the cylindrical vesicle that lies between L2 and the posterior singlet in *A. sigmoides*, although in the latter, the cylindrical vesicle does not actually appear to be adpressed to L2.

In typical excavates there is usually a single main anterior root, which usually originates on the anterior-dorsal side of the basal body, and most often curves to run down the left side of the cell (Park et al. 2009; Simpson 2003; Simpson et al. 2000). In many cases this root consists of a small number of microtubules (1–2, especially in small cells: O'Kelly and Nerad 1999; Simpson and Patterson 1999; Yubuki et al. 2007). There is therefore similarity between the typical excavate anterior root and the anterior root of *Ancyromonas sigmoides* in position and direction, and both (can) consist of a small number of microtubules. Typical excavates do not usually have a second anterior root to compare to the anterior singlet of *Ancyromonas*, although short 'protoroots' are found in a few excavates (Bernard et al. 1997; Simpson and Patterson 1999; Simpson et al. 2000) that might be homologous.

While there is notable similarity in the cytoskeletons of *Ancyromonas* and typical excavates, this should not be over-interpreted as strong evidence for a specific relationship. In particular, both the splitting crescent root/right root and the posterior singlet root may not be particular to *Ancyromonas*, apusomonads, and excavates. In bicosoecid stramenopiles, for example, the equivalent of the crescent root/right root (R2 - all bicosoecid terminology is sensu Moestrup 2000) also splits into two main components. Furthermore, the bicosoecid S tubule is very similar to the posterior singlet in the location of its origin, and it runs immediately alongside, and is connected to, the R1 root (see Karpov et al. 2001; Moestrup and Thomsen 1976; Yubuki et al. 2010). The bicosoecid R1 is the positional equivalent of the *Ancyromonas* L1, so this alignment of the S tubule is very similar to the posterior singlet of *Ancyromonas*. We therefore find that, while the position and nature of flagellar roots can be interpreted as being similar in *Ancyromonas* and excavates, these features may not indicate any specific evolutionary relationship.

During review of this paper, Cavalier-Smith and Chao (2010) independently noted similarities in the cytoskeletons of apusomonads, typical excavates, and bicosoecids. The reader is directed to this work for a similar view, though some of the root homologies proposed for apusomonads and these other taxa by Cavalier-Smith and Chao (2010) differ from those inferred here.

Summary and Conclusions

This updated account of the flagellar apparatus of *Ancyromonas* shows that it shares some similarity with *Apusomonas*, the best studied of its likely close relatives. Similarity is seen especially in the elements that originate around the posterior basal body (Table 1; Fig. 10). However, most of the cytoskeletal similarities between *Ancyromonas* and *Apusomonas* are also present in 'typical excavates' (Table 1; Fig. 10), and likely some other taxa that are very distantly related to *Ancyromonas* (see above). Thus the shared presence of possibly homologous features, such as a splitting root supporting the right side of the posterior flagellar groove/channel, and a posterior singlet root, is not in and of itself strong evidence for the monophyly of Apusozoa.

It is possible that some of these similarities may represent convergences. Another possibil-

Table 1. Comparison of ultrastructural features of *Ancyromonas*, *Apusomonas*, and 'typical excavates'.

Feature of *Ancyromonas sigmoides* strain B-70	Corresponding feature of *Apusomonas proboscidea* (Karpov 2007)	Corresponding feature of 'typical excavates' (Simpson 2003)
Crescent structure and associated roots (L2, L3)	Rhizostyle plus right posterior root	Right root (which splits into inner and outer ribbons)
L1 root	Two of the 'left posterior microtubules'	Left root
Posterior singlet root	Third left posterior microtubule	Singlet root
Anterior doublet	Dorsal root	Anterior root

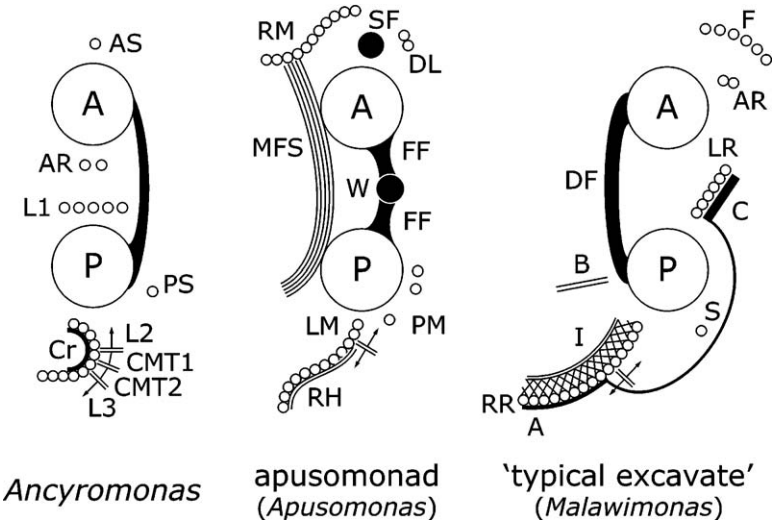

Figure 10. Diagrammatic comparison of the flagellar apparatus of *Ancyromonas sigmoides*, *Apusomonas proboscidea*, and a 'typical excavate' (represented by *Malawimonas jakobiformis*), using the technique of Sleigh (1988). Both basal bodies (all organisms depicted being biflagellated) are viewed from tip to base, and each is imagined to be rotated, without torsion along the flagellar axis, along with its associated cytoskeletal elements, so as to be parallel to the other. [A] indicates the anterior basal body, [P] the posterior; the smaller circles each indicate microtubules. Lines indicate nonmicrotubular structures. Split arrows indicate microtubular structures that bifurcate at some point. Note that not all structures may be extant within the same plane. Abbreviations for *Ancyromonas*: [CMT1] and [CMT2]: crescent microtubules 1 and 2, respectively; all others are as elsewhere in the text. Orientation for *Ancyromonas*: dorsal is to the right, medial to the centreline. Abbreviations for *Apusomonas*: [DL]: dorsal left microtubules; [FF]: fused feet; [LM]: left microtubular component of rhizostyle; [MFS]: multilayered fibrillar structure; [PM]: posterior left microtubules; [SF]: striated fibre; [RH]: rhizostyle; [RM]: right microtubules; [W]: wheel. Orientation for *Apusomonas*: dorsal is to the right, left lateral (for each flagellar system) is at the top. Abbreviations for *Malawimonas*: [A]: A fibre; [AR]: anterior root; [B]: B fibre; [C]: C fibre; [DF]: distal connecting fibre; [F]: dorsal fan; [I]: I fibre; [LR]: left posterior root; [RR]: right posterior root; [S]: singlet root. Ventral is at the centreline; the cell's left is to the viewer's right. *Apusomonas* prepared from data in Karpov (2007); *Malawimonas* adapted from figure in Simpson (2003) with reference to O'Kelly and Nerad (1999).

ity, however, is that such features may be deep plesiomorphies within eukaryotes, i.e. ancestral features for most or all living eukaryotes, which have been retained by certain lineages that may be distantly related to one another (see also Cavalier-Smith and Chao 2010). The very deep-branching positions within eukaryotes suspected for *Ancyromonas*, apusomonads, and excavates make this possibility more parsimonious than if they were highly nested within major groups, as fewer events of loss need to be inferred.

Two elements are particularly needed to improve our understanding of the relative positions and evolutionary importance of *Ancyromonas*, the apusomonads, and the excavates. Firstly, phylogenetic studies are required that include substantial data from *Ancyromonas*, apusomonads, and excavates at the same time. Secondly, detailed studies of apusomonad ultrastructure (particularly that of the less-derived members of the group) are required to bring our knowledge of this group up to the level of detail now available for *Ancyromonas* and typical excavates. In combination, these two approaches could well allow us to resolve some of the deepest-level relationships amongst eukaryotes, and to reconstruct the nature of the shared ancestors of the various eukaryotic 'supergroups', possibly extending even to the common ancestor of all extant eukaryotic cells.

Methods

Liquid cultures of *Ancyromonas sigmoides* (syn. *Planomonas mylnikovi*) strain B-70 of Mylnikov, CCAP 1958/3 (Cavalier-Smith et al. 2008; Heiss et al. 2010; Mylnikov 1990) were observed by light microscopy using a 100x oil-immersion objective with a 1.6x "optovar" magnifier and phase-contrast optics. Images were captured using a Zeiss Axiocam HR 1.4-megapixel digital camera.

Prior to fixation for TEM, cells were pelleted by centrifugation at 3,000 × *g* for 20 minutes. They were then transferred to 200-μm-deep brass planchettes that had been previously coated in

hexadecene and allowed to dry. Each planchette was covered with another of the same depth, flat side opposed to the cavity containing the specimen. The samples were high-pressure frozen using a BAL-TEC HPM 010 High Pressure Freezer. Specimens, still in planchettes, were transferred to microporous pots under liquid nitrogen, and covered with frozen HPLC-grade acetone. The temperature of these was raised from -160 °C to -85 °C by 15 °C/hr and then held at -85 °C for 24 hours. The planchettes were transferred to fresh pots containing 2% OsO4 and 0.1% glutaraldehyde in HPLC-grade acetone, and kept for a further 26 hours at -85 °C. Specimens were warmed by 2 °C/hr to -30 °C, being held at -60 °C for 8 hours and at -30 °C for 24.5 hours, and subsequently by 1 °C/hr to -20 °C, at which point they were transferred first to a -20 °C freezer and then to a 4 °C refrigerator, each for 24 hours. After this, they were allowed to warm to room temperature in a fume hood for 4 hours, subjected to three washes of 100% acetone for 20 minutes each, and removed from their planchettes. Specimens were subjected to a 10%–25%–50%–75% series of TAAB resin in acetone for 2 hours each before being transferred through 10 changes of 100% TAAB resin, each pure resin change lasting 12 hours except for the second, which was for 8 hours. The resin was polymerised at 70 °C for 24 hours. Blocks were sectioned at 70 and 50 nm thicknesses on an ultramicrotome. Ribbons were mounted on 2 mm slot grids and placed on 40-60 nm thick pioloform film using the method of Rowley and Moran (1975). Grids were stained using a saturated uranyl acetate solution in 50% (v/v) ethanol for 1 minute and Reynold's lead citrate for 2 minutes.

Transmission electron microscopy was performed on an electron microscope fitted with a rotating specimen holder and a tilting stage (with which tilt angles up to 35° were employed). Specimen images were observed, and series from eight cells (20-30 sections each) captured, with a 1-megapixel digital camera. Series were aligned along one or both of the two basal bodies. We captured additional images from single sections, as well as shorter, unaligned series, from other cells. Some individual images were captured on 4- and 11-megapixel cameras. For two of the series (one aligned with each of the two basal bodies), we manually annotated the digital images using a drawing program, and imported the vector data from the annotated images into a 3D modelling program, with which models were constructed. These models were compared with one another, and corrections were made by reference to unmodelled series.

Acknowledgements

The authors thank Alexander P. Mylnikov, for originally isolating the strain used in this study, and Ema Chao and Tom Cavalier-Smith (University of Oxford), for providing that strain to us. We also thank Barry Martin, in the Plant Cell Biology research facility at Oxford Brookes University, for fixation, dehydration, and embedding of specimens. Ping Li, of the Scientific Imaging Suite in the Dalhousie Faculty of Science, and Mary Ann Trevors, of the Electron Microscopy Facility in the Dalhousie Faculty of Medicine, provided assistance with TEM operations. Alaric Heiss provided invaluable guidance for the computer-based reconstruction. Yana Eglit kindly translated the Russian primary literature for us. We thank Gillian Gile, Michelle Leger, and Yana Eglit for thoughtful commentary and advice anent the manuscript. This work is supported by NSERC grant 298366-04 to AGBS, and the Canadian Institute for Advanced Research (CIfAR) program in Integrated Microbial Biodiversity. GW received funding from the Linnean Society and the Systematics Association's CoSyst scheme, and a short travel grant from the Royal Society. AAH is supported in part by a Dalhousie University Faculty of Graduate Studies scholarship.

Appendix A. Supplementary data

Supplementary data associated with this article can be found, in the online version, at doi:10.1016/j.protis.2010.08.004.

References

Adl SM, Simpson AGB, Farmer MA, Andersen RA, Anderson OR, Barta JR, Bowser SS, Brugerolle G, Fensome RA, Fredericq S, James TY, Karpov S, Kugrens P, Krug J, Lane CE, Lewis LA, Lodge J, Lynn DH, Mann DG, McCourt RM, Mendoza L, Moestrup Ø, Mozley-Standbridge SE, Nerad TA, Shearer CA, Smirnov AV, Spiegel FW, Taylor FJR (2005) The new higher level classification of eukaryotes with emphasis on the taxonomy of protists. J Eukaryot Microbiol **52**:399–451

Arisue N, Hasegawa M, Hashimoto T (2005) Root of the Eukaryota tree as inferred from combined maximum likelihood analyses of multiple molecular sequence data. Mol Biol Evol **22**:409–420

Atkins MS, McArthur AG, Teske AP (2000a) Ancyromonadida: a new phylogenetic lineage among the protozoa closely related to the common ancestor of metazoans, fungi, and choanoflagellates (Opisthokonta). J Mol Evol **51**:278–285

Atkins MS, Teske AP, Anderson OR (2000b) A survey of flagellate diversity at four deep-sea hydrothermal vents in the eastern pacific ocean using structural and molecular approaches. J Eukaryot Microbiol **47**:400–411

Baldauf SL (2003) The deep roots of eukaryotes. Science **300**:1703–1706

Bernard C, Simpson AGB, Patterson DJ (1997) An ultrastructural study of a free-living retortamonad, *Chilomastix cuspidata* (Larsen & Patterson 1990) n. comb (Retortamonadida, Protista). Eur J Protistol **33**:254–265

Brugerolle G (2002) *Cryptophagus subtilis*: a new parasite of cryptophytes affiliated with the Perkinsozoa lineage. Eur J Protistol **37**:379–390

Burki F, Shalchian-Tabrizi K, Pawlowski J (2008) Phylogenomics reveals a new "megagroup" including most photosynthetic eukaryotes. Biol Lett **4**:366–369

Burki F, Shalchian-Tabrizi K, Minge M, Skjaeveland A, Nikolaev SI, Jakobsen KS, Pawlowski J (2007) Phylogenomics reshuffles the eukaryotic supergroups. PLoS ONE **2**:e790

Cavalier-Smith T (2002) The phagotrophic origin of eukaryotes and phylogenetic classification of Protozoa. Int J Syst Evol Microbiol **52**:297–354

Cavalier-Smith T (2003) The excavate protozoan phyla Metamonada Grassé emend (Anaeromonadea, Parabasalia, *Carpediemonas*, Eopharyngia) and Loukozoa emend (Jakobea, *Malawimonas*): Their evolutionary affinities and new higher taxa. Int J Syst Evol Microbiol **53**:1741–1758

Cavalier-Smith T (2009) Megaphylogeny, cell body plans, adaptive zones: causes and timing of eukaryote basal radiations. J Eukaryot Microbiol **56**:26–33

Cavalier-Smith T, Chao EE (1995) The opalozoan *Apusomonas* is related to the common ancestor of animals, fungi, and choanoflagellates. Proc Roy Soc London B **261**:1–6

Cavalier-Smith T, Chao EE (2003) Phylogeny of Choanozoa, Apusozoa, and other protozoa and early eukaryote megaevolution. J Mol Evol **56**:540–563

Cavalier-Smith T, Chao EE (2010) Phylogeny and evolution of Apusomonadida (Protozoa: Apusozoa): new genera and species. Protist **161**:549–576

Cavalier-Smith T, Chao EE, Oates B (2004) Molecular phylogeny of Amoebozoa and the evolutionary significance of the unikont *Phalansterium*. Eur J Protistol **40**:21–48

Cavalier-Smith T, Chao EE, Stechmann A, Oates B, Nikolaev S (2008) Planomonadida ord. nov. (Apusozoa): ultrastructural affinity with *Micronuclearia podoventralis* and deep divergences within *Planomonas* gen. nov. Protist **159**: 535–562

Foissner I, Foissner W (1993) Revision of the family Spironemidae Doflein (Protista, Hemimastigophora), with description of two new species, *Spironema terricola* n. sp. and *Stereonema geiseri* n. g., n. sp. J Eukaryot Microbiol **40**:422–438

Foissner W, Blatterer H, Foissner I (1988) The Hemimastigophora (*Hemimastix amphikineta* nov. gen., nov. spec.), a new protistan phylum from Gondwanian soils. Eur J Protistol **23:**:361–383

Hampl V, Hug L, Leigh JW, Dacks JB, Lang BF, Simpson AGB, Roger AJ (2009) Phylogenomic analyses support the monophyly of Excavata and resolve relationships among eukaryotic "supergroups". Proc Natl Acad Sci USA **106**:3859–3864

Heiss AA, Walker G, Simpson AGB (2010) Clarifying the taxonomic identity of a phylogenetically important group of eukaryotes: *Planomonas* is a junior synonym of *Ancyromonas*. J Eukaryot Microbiol **57**:273–284

Hippe S, Hermanns M (1986) Improved structural preservation in freeze-substituted sporidia of *Ustilago avenae* — a comparison with low-temperature embedding. Protoplasma **135**: 19–30

Karpov SA (1990) System of Protists. Omsk, Mezhvuzoskaya (in Russian)

Karpov SA (2007) The flagellar apparatus structure of *Apusomonas proboscidea* and apusomonad relationships. Protistology **5**:146–155

Karpov SA, Mylnikov AP (1989) Biology and ultrastructure of colourless flagellates Apusomonadida ord. n. Zool Zh **68** (8): 5–17 (in Russian)

Karpov SA, Zhukov BF (1984) Ultrathin structure of the colourless flagellate *Apusomonas proboscidea*. Tsitologiya **26**: 886–890 (In Russian)

Karpov SA, Zhukov BF (1986) Ultrastructure and taxonomic position of *Apusomonas proboscidea* Alexeieff. Arch Protistenkd **131**:13–26

Karpov SA, Sogin ML, Silberman JD (2001) Rootlet homology, taxonomy, and phylogeny of bicosoecids based on 18S rRNA gene sequences. Protistology **2**:34–47

Keeling PJ, Burger G, Durnford DG, Lang BF, Lee RW, Pearlman RE, Roger AJ, Gray MW (2005) The tree of eukaryotes. Trends Ecol Evol **20**:670–676

Kim E, Simpson AGB, Graham LE (2006) Evolutionary relationships of apusomonads inferred from taxon-rich analyses of six nuclear-encoded genes. Mol Biol Evol **23**:2455–2466

Lancelle SA, Callaham DA, Hepler PK (1986) A method for rapid freeze fixation of plant cells. Protoplasma **131**:153–165

Marande W, López-García P, Moreira D (2009) Eukaryotic diversity and phylogeny using small- and large-subunit ribosomal RNA genes from environmental samples. Environ Microbiol **11**:3179–3188

Mikrjukov KA, Mylnikov AP (2001) A study of the fine structure and the mitosis of a lamellicristate amoeba, *Micronuclearia podoventralis* gen. et sp. nov (Nucleariidae, Rotosphaerida). Eur J Protistol **37**:15–24

Minge MA, Silberman JD, Russell JS, Orr RJS, Cavalier-Smith T, Shalchian-Tabrizi K, Burki F, Skjæveland Å, Jakobsen KS (2009) Evolutionary position of breviate amoebae and the primary eukaryote divergence. Proc Roy Soc B **276**:597–604

Moestrup Ø (2000) The Flagellate Cytoskeleton. In Leadbeater BSC, Green JC (eds) The Flagellates: Unity, Diversity and Evolution. Taylor and Francis, London, pp 69–94

Moestrup Ø, Thomsen HA (1976) Fine structural studies on the flagellate genus *Bicoeca*. I. *Bicoeca maris* with particular emphasis on the flagellar apparatus. Protistologica **12**:101–120

Molina FI, Nerad TA (1991) Ultrastructure of *Amastigomonas bermudensis* ATCC 50234 sp. nov. Eur J Protistol **27**:386–396

Mylnikov AP (1989) Ultrathin structure of flagellate *Amastigomonas caudata*. Tsitologiya **31**: 567-571 (in Russian)

Mylnikov AP (1990) Characteristic features of the ultrastructure of colourless flagellate *Heteromita* sp. Tsitologiya **32**: 567-570 (in Russian)

O'Kelly CJ, Nerad TA (1999) *Malawimonas jakobiformis* n. gen., n. sp (Malawimonadidae n. fam.): A *Jakoba*-like heterotrophic nanoflagellate with discoidal mitochondrial cristae. J Eukaryot Microbiol **46**:522–531

Parfrey LW, Barbero E, Lasser E, Dunthorn M, Bhattacharya D, Patterson DJ, Katz LA (2006) Evaluating support for the current classification of eukaryotic diversity. PLoS Genetics **12**:2062–2073

Park JS, Kolisko M, Heiss AA, Simpson AGB (2009) Light microscopic observations, ultrastructure, and molecular phylogeny of *Hicanonectes teleskopos* n. g., n. sp., a deep-branching relative of diplomonads. J Eukaryot Microbiol **56**:373–384

Patterson DJ (1999) The diversity of eukaryotes. Am Nat **65** (Suppl): S96–S124

Patterson DJ, Vørs N, Simpson AGB, O'Kelly C (2000) Residual Free-Living and Predatory Heterotrophic Flagellates. In Lee JJ, Leedale GF, Bradbury P (eds) The Illustrated Guide to the Protozoa, 2nd ed. Society of Protozoologists, Lawrence, Kansas, pp 1302–1328

Richards TA, Cavalier-Smith T (2005) Myosin domain evolution and the primary divergence of eukaryotes. Nature **436**:1113–1118

Roger AJ, Simpson AGB (2009) Evolution: Revisiting the root of the eukaryote tree. Curr Biol **24**:R165–R167

Rowley III JC, Moran DT (1975) A simple procedure for mounting wrinkle-free sections on Formvar-coated slot grids. Ultramicroscopy **1**:151–155

Simpson AGB (2003) Cytoskeletal organization, phylogenetic affinities and systematics in the contentious taxon Excavata (Eukaryota). Int J Syst Evol Microbiol **53**: 1759–1777

Simpson AGB, Patterson DJ (1999) The ultrastructure of *Carpediemonas membranifera* (Eukaryota), with reference to the 'excavate hypothesis'. Eur J Protistol **35**:353–370

Simpson AGB, Patterson DJ (2001) On core jakobids and excavate taxa: the ultrastructure of *Jakoba incarcerata*. J Eukaryot Microbiol **48**:480–492

Simpson AGB, Roger AJ (2004) The real 'kingdoms' of eukaryotes. Curr Biol **14**:R693–R696

Simpson AGB, Bernard C, Patterson DJ (2000) The ultrastructure of *Trimastix marina* Kent, 1880 (Eukaryota), an excavate flagellate. Eur J Protistol **36**:229–251

Sleigh MA (1988) Flagellar root maps allow speculative comparisons of root patterns and their ontogeny. BioSystems **21**:277–282

Stechmann A, Cavalier-Smith T (2002) Rooting the eukaryote tree by using a derived gene fusion. Science **297**:89–91

Stechmann A, Cavalier-Smith T (2003) The root of the eukaryote tree pinpointed. Curr Biol **13**:R665–R666

Yoon HS, Grant J, Tekle YI, Wu M, Chaon BC, Cole JC, Logsdon JMJr, Patterson DJ, Bhattacharya D, Katz LA (2008) Broadly sampled multigene trees of eukaryotes. BMC Evol Biol **8**:14

Yubuki N, Leander BS, Silberman JD (2010) Ultrastructure and molecular phylogenetic position of a novel phagotrophic stramenopile from low oxygen environments: *Rictus lutensis* gen. et sp. nov. (Bicosoecida, incertae sedis). Protist **161**:264–278

Yubuki N, Inagaki Y, Nakayama T, Inouye I (2007) Ultrastructure and ribosomal RNA phylogeny of the free-living heterotrophic flagellate *Dysnectes brevis* n. gen., n. sp., a new member of the Fornicata. J Eukaryot Microbiol **54**:191–200